

Crystal structures of truncated alphaA and alphaB crystallins reveal structural mechanisms of polydispersity important for eye lens function

Arthur Laganowsky,^{1,2} Justin L. P. Benesch,^{3,4} Meytal Landau,^{1,2} Linlin Ding,⁵ Michael R. Sawaya,¹ Duilio Cascio,^{1,2} Qingling Huang,⁵ Carol V. Robinson,^{3,4} Joseph Horwitz,⁵ and David Eisenberg^{1,2*}

¹Howard Hughes Medical Institute, UCLA-DOE Institute for Genomics and Proteomics, Los Angeles, California

²Department of Chemistry and Biochemistry, University of California Los Angeles, Los Angeles, California

³Physical and Theoretical Chemistry Laboratory, Department of Chemistry, University of Oxford, Oxford OX1 3QZ, United Kingdom

⁴Department of Chemistry, University of Cambridge, Cambridge CB2 1EW, United Kingdom

⁵Jules Stein Eye Institute, University of California Los Angeles, Los Angeles, California

Received 22 December 2009; Revised 1 March 2010; Accepted 1 March 2010

DOI: 10.1002/pro.380

Published online 29 March 2010 proteinscience.org

Abstract: Small heat shock proteins alphaA and alphaB crystallin form highly polydisperse oligomers that frustrate protein aggregation, crystallization, and amyloid formation. Here, we present the crystal structures of truncated forms of bovine alphaA crystallin (AAC_{59–163}) and human alphaB crystallin (ABC_{68–162}), both containing the C-terminal extension that functions in chaperone action and oligomeric assembly. In both structures, the C-terminal extensions swap into neighboring molecules, creating runaway domain swaps. This interface, termed DS, enables crystallin polydispersity because the C-terminal extension is palindromic and thereby allows the formation of equivalent residue interactions in both directions. That is, we observe that the extension binds in opposite directions at the DS interfaces of AAC_{59–163} and ABC_{68–162}. A second dimeric interface, termed AP, also enables polydispersity by forming an antiparallel beta sheet with three distinct registration shifts. These two polymorphic interfaces enforce polydispersity of alpha crystallin. This evolved polydispersity suggests molecular mechanisms for chaperone action and for prevention of crystallization, both necessary for transparency of eye lenses.

Keywords: X-ray diffraction; small heat shock protein; protein chaperone; desmin-related myopathy; cataract; eye lens transparency

Abbreviations: AAC_{59–163}, alphaA crystallin residues 59–163; AAC_{59–163}-Zn, zinc-bound alphaA crystallin residues 59–163; ABC_{68–162}, alphaB crystallin residues 68–162; ABC_{68–157}, alphaB crystallin residues 68–157; ABC_{67–157}, alphaB crystallin residues 67–157; ADH, alcohol dehydrogenase; AP, antiparallel beta sheet interface; AP_x, antiparallel beta sheet registration state x; DS, domain-swapped interface; Hsp20_{65–162}, rat heat shock protein 20 residues 65–162; MjHsp16.5, *Methanococcus janaschii* heat shock protein 16.5; MS, mass spectrometry; sHSP, small heat shock protein; WhHsp16.9, wheat heat shock protein 16.9.

Additional Supporting Information may be found in the online version of this article.

Grant sponsor: NIH Chemistry Biology Interface Training Program; Grant number: 5T32GM008496; Grant sponsor: DOE BER; Grant number: DE-FC02-02ER63421, DE-AC02-05CH11231, DE-AC02-06CH11357; Grant sponsor: NIH National Center for Research Resources; Grant number: RR-15301; Grant sponsors: NSF; the Royal Society; HHMI; NIH National Eye Institute; Grant number: EY 3897.

*Correspondence to: David Eisenberg, Howard Hughes Medical Institute, UCLA-DOE Institute for Genomics and Proteomics, Los Angeles, CA 90095-1570. E-mail: david@mbi.ucla.edu

Introduction

Alpha crystallin is a major protein component of the vertebrate eye lens, where its high density and solubility contribute to the refractive function of this organ. As members of the small heat shock family of proteins, alphaA crystallin (AAC) and alphaB crystallin (ABC) provide a chaperone barrier to protein misfolding and aggregation in eye lens and other tissues. As recently reviewed by McHaourab *et al.*,¹ numerous studies have shown that the alpha crystallins recognize and bind destabilized proteins, preventing protein aggregation and amyloid fibril formation.^{2–6} Related to its chaperone function, ABC accumulates in many diseases (for review see Refs. 7–9): Creutzfeldt-Jakob disease,¹⁰ Alexander disease,¹¹ diffuse Lewy body disease,¹² Parkinson's disease,¹³ and Alzheimer's disease.¹⁴ In several cases, ABC colocalizes with the amyloid-like protein deposits.⁷ The colocalization and overexpression of ABC in deposition diseases suggest its beneficial cellular role in countering initial unfolding and in overcoming aberrant accumulation of disease-related proteins.

Alpha crystallins and other members of the small heat shock protein family^{15–17} assemble into polydisperse and dynamic oligomers.^{18,19} AAC and ABC with sequence identity of about 57%²⁰ form polydisperse oligomers, which may explain why the untruncated molecules have long resisted crystallization. The oligomeric state is not only variable, with AAC and ABC populating ensembles with means of 26 and 28 subunits, respectively,²¹ but also dynamic, with subunits exchanging freely to form a range of heterooligomers.²² Cryoelectron microscopic studies have also shown human ABC oligomers to have a variable quaternary structure and to be generally roughly spherical, with a central cavity.²³ Recent single-particle analysis has enabled the reconstruction of a sphere-like structure of ABC, which is composed of 24 subunits.²⁴ The polydisperse nature of the alpha crystallins has been suggested to be important for chaperone function^{20–22,25} and has been shown to be related to the N-terminal region of the proteins.¹⁹

A long period of frustration in growing crystals of the alpha crystallins has been bypassed by truncation of terminal segments by Bagneris *et al.*²⁶ and independently by us. Bagneris *et al.*²⁶ determined structures of truncated alpha crystallin domains from rat and human. The rat domain (here termed Hsp20_{65–162}) comprises residues 65–162, and the human domain (ABC_{67–157}) comprises residues 67–157.²⁶ Both form dimers through an antiparallel beta sheet.²⁶ The authors note that the registration of this antiparallel beta sheet interface is different in their two structures, perhaps contributing to polydispersity of the crystallins. This antiparallel beta-sheet interaction was suggested previously by site-

directed labeling EPR studies and by hybrid solid-state/solution-state NMR.^{27–30}

The structures reported here extend the information provided by the structures of Bagneris *et al.*²⁶ They offer electron density for the important residues 151–157, which the ABC_{67–157} structure lacks, and also offer the structure of the highly conserved C-terminal tail sequence IPI/V, which illuminates one factor in maintenance of lens transparency.

Related structures of other members of the small heat shock protein (sHSP) family^{15–17} have been determined: for Wheat Hsp16.9 (WhHsp16.9),³¹ *Methanococcus janaschii* Hsp16.5 (MjHsp16.5),³² *Xanthomonas axonopodis* HspA,³³ and Metazoan Tsp36.³⁴ The structure of the conserved C-terminal extension that we find important for enforcing polydispersity has been observed only in WhHsp16.9³¹ and MjHsp16.5.³² In these structures, the C-terminal extension binds to a groove in the conserved alpha crystallin domain of an adjacent chain, linking together specific chaperone assemblies. In the MjHsp16.5, 24 monomers make up the hollow open shell-like chaperone complex, where the C-terminal extension is involved in interlocking four- and three-fold oligomeric units together.³² In the WhHsp16.9 structure, a hinge loop consisting of residues 137–144 allows two different binding modes, which vary by 30°, involved in stabilizing the double disk-like chaperone complex composed of 12 chains.³¹ The hinge loop variability allows two C-terminal extension binding modes, where it interlocks within each disk and between the disks to form the double disk assembly.³¹ In both of these structures, the C-terminal extensions decorate the outside of the chaperone assemblies, suggesting a possible role in assembly, disassembly, and chaperone activity.

Results

Truncated AAC and ABC structures reveal the immunoglobulin-like, beta sandwich fold formed with seven beta strands (Fig. 2). We achieved crystallization by removing 59 and 68 N-terminal residues and 10 and 13 C-terminal residues from AAC and ABC, respectively (Table I). These truncated proteins are termed AAC_{59–163} and ABC_{68–162}. The beta sandwich fold of the alpha crystallin domain is similar to the crystal structures of ABC_{67–157}²⁶ and Hsp20_{65–162},²⁶ EPR spin-labeled structure of AAC alpha crystallin domain,³⁵ and to the eight beta strand containing beta sandwich cores of MjHsp16.5,³² WhHsp16.9,³¹ Tsp36,³⁴ and HspA.³³ More generally, the overall architecture is similar to the beta and gamma crystallin double greek key motif.³⁶ In the AAC_{59–163} and ABC_{68–162} structures, one side of the beta sandwich consists of three beta strands that form an antiparallel beta sheet interaction at the dimer interface, which we term the AP interface. The AP

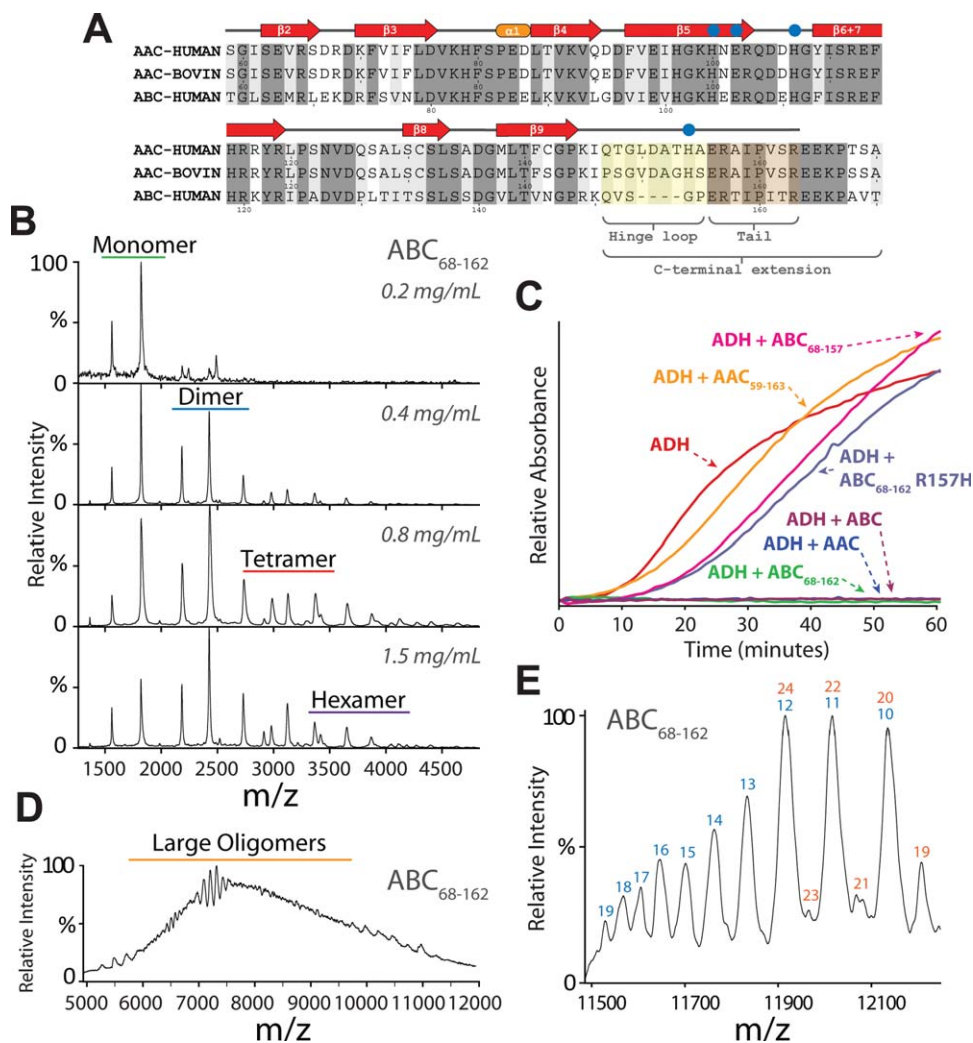


Figure 1. Truncated alphaA and alphaB crystallin constructs (AAC₅₉₋₁₆₃ and ABC₆₈₋₁₆₂) amino acid sequence alignment, chaperone-like activity, and concentration-dependent molecular mass. (A) Human and bovine alphaA crystallin (AAC) and human alphaB crystallin (ABC) amino acid sequence alignment. Residue numbers for AAC and ABC are listed at the bottom. Beta-strand assignments are labeled, and AAC residues involved in zinc binding (blue circles) are above amino acid sequence. Amino acid similarity is shaded in gray; dark gray indicates identical residues, and light gray indicates the chemically similar residues. The C-terminal hinge loop (shaded in yellow) and tail are labeled. The C-terminal tail palindromic sequence is shaded in orange. (B) Nanoelectrospray MS reveals a concentration-dependent molecular mass, consisting of monomers, dimers, tetramers, and hexamers. Each panel represents a mass spectrum at different protein concentrations for ABC₆₈₋₁₆₂. Located on the right of each mass spectrum is the protein concentration used in the injection. Lines, at the top, highlight the ion series corresponding to a molecular mass of a monomer, dimer, tetramer, and hexamer. At low protein concentrations, the main molecular mass is a monomer (top panel), whereas at higher protein concentrations the molecular mass shifts from a monomer to a distribution of dimer, tetramer, and hexamer (bottom panel). (C) Protein aggregation of alcohol dehydrogenase (ADH) was monitored by absorbance at 360 nm, and aggregation induced by heating to 37°C (red line). AAC (dark blue line), ABC (violet line), and ABC₆₈₋₁₆₂ (green line) prevented ADH protein aggregation displaying chaperone-like activity. AAC₅₉₋₁₆₃ (orange line), mutant ABC₆₈₋₁₆₂ R157H (blue line), and ABC₆₈₋₁₅₇ (pink line) displayed no chaperone-like activity. (D) Despite the preponderance of suboligomeric species (B), large polydisperse oligomers can still be observed for AAC₅₉₋₁₆₃ and ABC₆₈₋₁₆₂. To interrogate this unresolved area of signal, we perform tandem MS. (E) Collision-induced dissociation of the oligomers (Supporting Information Fig. S3). The number in blue or red corresponds to oligomer size carrying $n - 1$ or $n - 2$ charges, respectively. The large oligomers range in size from 10 to 24 subunits.

interface generates one side with a surface composed of six beta strands. Extending away from the seven beta strand core domain is what we term the C-terminal extension (see below). The C-terminal extension binds to the top of the beta sandwich of another molecule.

We define the two subsegments that make up the C-terminal extension in our truncated constructs as the hinge loop and C-terminal tail [Fig. 1(A)]. The C-terminal tail is the part of the C-terminal extension containing the highly conserved I-X-I/V sequence that binds to an adjacent chain. The hinge

loop is the linker between the alpha crystallin core and C-terminal tail. The C-terminal tail of ABC contains a palindromic sequence.²⁶ As described below, we find bidirectional binding of the C-terminal extension for AAC and ABC, permitted by the conserved palindromic sequence.

In the full-length alpha crystallins, the conserved C-terminal extension has been implicated in both substrate recognition and chaperone action. Mutations in the C-terminal tail display either reduced or enhanced chaperone-like activity depending on protein substrate.^{6,37,38} Deletion of the C-terminal extension in ABC leads to a reduction in chaperone activity, an increase in polydispersity, and an increase in oligomeric size.³⁹ The C-terminal extension functions in recognition and selection of unfolded protein substrates.³⁹

Properties of truncated alpha crystallins

Chaperone-like activity for various alpha crystallin constructs were evaluated using alcohol dehydrogenase (ADH), insulin, lactalbumin, lysozyme, and ovotransferrin as target proteins. AAC and ABC displayed chaperone-like activity for all target proteins tested [Fig. 1(C) and Supporting Information Fig. S1]. The ABC_{68–162} proteins exhibit chaperone-like activity for ADH and moderate chaperone-like activity for lactalbumin (Fig. 1(C) and Supporting Information Fig. S1). The AAC_{59–163}, mutant ABC_{68–162} R157H, and ABC_{68–157} (construct containing residues 68–157) proteins displayed no chaperone-like activity for target proteins tested (Supporting Information Fig. S1). In some cases, the truncated constructs precipitated with the target proteins. In short, ABC_{68–162} displays some chaperone activity verifying that this structure has relevance for understanding chaperone function.

AAC_{59–163} and ABC_{68–162} proteins exhibit a concentration-dependent molecular weight similar to those of full-length AAC and ABC. As concentration increases, the average light scattering mass increases from a dimer (20 kDa) to trimer (35 kDa) and then to a tetramer (40 kDa) (Supporting Information Fig. S2). The overall shape of the light scattered mass indicates slight polydispersity. Nanoelectrospray mass spectrometry (MS) was used to examine the concentration-dependent molecular mass at higher resolution [Fig. 1(B) and Supporting Information Fig. S3(A)]. The main species at lower protein concentrations is a monomer, whereas at higher protein concentrations the species distribution ranges from dimers to tetramers and hexamers. Despite the dominance of these suboligomeric species, by tuning our mass spectrometer to favor the transmission of high mass species, we can clearly detect signal corresponding to a polydisperse ensemble of large oligomers [Fig. 1(D)]. Such a spectrum is not interpretable by MS alone but can be deconvoluted

into the individual components by performing tandem MS.¹⁸ By sequentially removing two monomers by gas-phase dissociation, the charge on the resultant oligomers has been reduced such that individual species can be resolved.⁴⁰ We find that for all the constructs, oligomers in the range from 10 to 24 molecules can be detected, with oligomers containing an even number of monomers being slightly favored over those with an odd number [Supporting Information Fig. S3 and Fig. 1(E)]. This observed wide range of oligomer stoichiometries in solution is consistent with the variety of intermolecular contacts that we observe in our crystal structures.

C-terminal hinge loop flexibility

The AAC C-terminal hinge loop exhibits structural flexibility in two crystal structures. In the first AAC_{59–163} structure, the flexible hinge loop allows the C-terminal tail to bind to neighboring molecules (Fig. 2). No electron density was observed for part of the hinge loop, and the distance between C α s of residues 151 and 156 is 12 Å, which could accommodate the unmodeled five residues. In a second AAC_{59–163} crystal structure, the hinge loop participates in zinc binding (AAC_{59–163}-Zn), discussed below (Fig. 3 and Supporting Information Fig. S4). The C-terminal extension differs in direction for the two AAC_{59–163} structures while maintaining the same C-terminal tail orientation (Supporting Information Fig. S5). Other than the difference in C-terminal extension direction, the AAC_{59–163} and AAC_{59–163}-Zn structures are very similar giving a C α backbone RMSD of ~ 0.2 Å for residues 61–146.

The ABC_{68–162} C-terminal extensions swap into neighboring molecules. A dimeric interface is created by the domain swap of this C-terminal extension (Fig. 4). The hinge loop within the C-terminal extension is four amino acids shorter for ABC_{68–162} than in AAC_{59–163} [Fig. 1(A)]. The shorter hinge loop of ABC_{68–162}, extends away from the crystallin core, roughly parallel to the beta strands of the core (Fig. 4).

AAC_{59–163} zinc-binding motif

A zinc-binding motif in AAC_{59–163} seems to aid oligomerization. In total three molecules form the zinc-binding motif [Figs. 1(A) and 3, inset]. A glutamate and histidine from one molecule are ligands of the zinc ion, and two histidine residues from additional molecules complete the site with tetrahedral coordination geometry. The C-terminal hinge loop adopts a “w” like structure (Supporting Information Fig. S4), composed of weaving beta hairpin structures, that positions a key histidine residue in the zinc-binding motif. A fourth histidine comes from the loop located between $\beta 5$ and $\beta 6 + 7$ [Fig. 1(A)]. These four residues involved in zinc binding have a similar architecture (within an RMSD of 3 Å) to roughly 1000

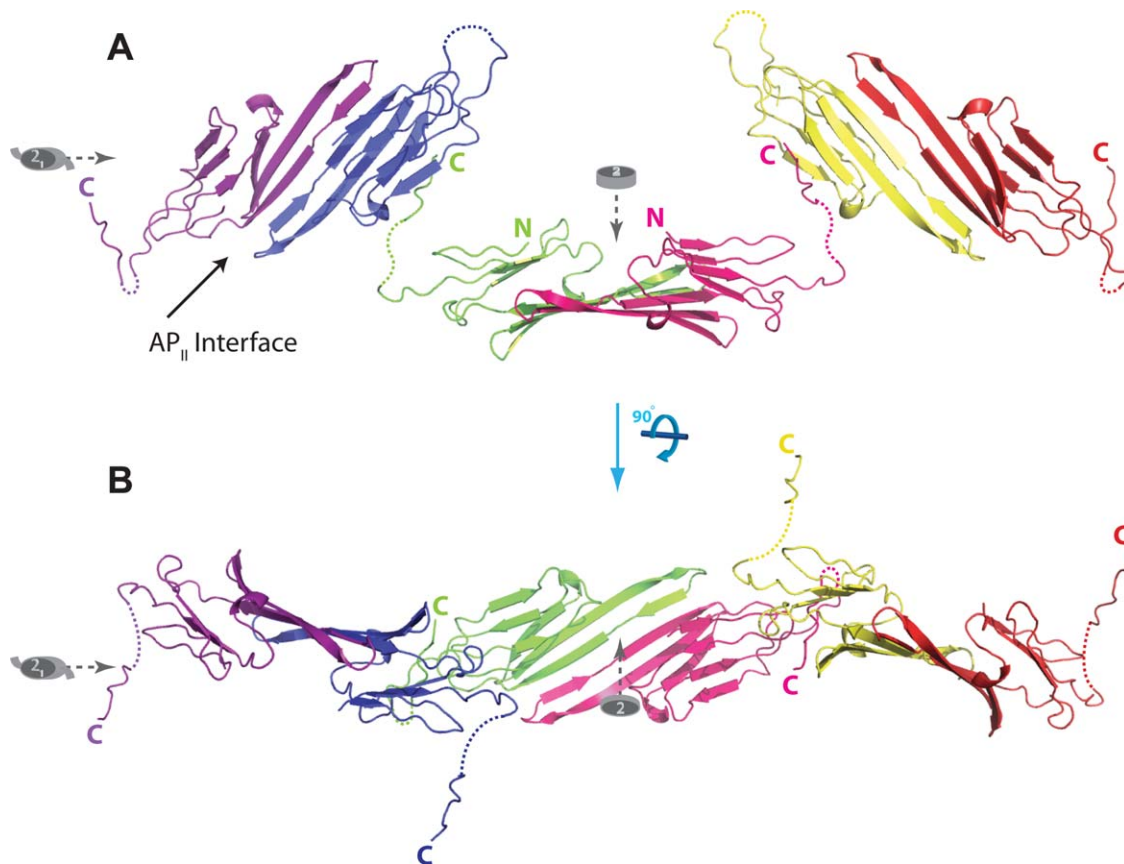


Figure 2. The crystal structure of AAC_{59–163} reveals C-terminal tail binding to adjacent chains. Twofold (ovals) and twofold screw (winged ovals) crystallographic axes are shown. The flexible hinge loop is shown by dashed lines, and termini labels are color coded for each chain. (A) The C-terminal extensions protrude from each end of the central dimer. The extended C-terminal extensions bind to adjacent dimers, which continue along the twofold screw axis. (B) The C-terminal extensions of the bound adjacent chains (colored blue and yellow) continue along differing twofold screw axes, interacting with differing adjacent dimers. An [interactive view](#) is available in the electronic version of the article.

Zn-binding sites in other proteins, as identified from a spatial motif search.⁴¹ ABC lacks one histidine residue, located in the hinge loop, of the zinc-binding motif observed in AAC_{59–163}-Zn [Fig. 1(A)].

Bidirectional binding of the C-terminal extension

Crystal structures of AAC_{59–163}, AAC_{59–163}-Zn, and ABC_{68–162} reveal bidirectional binding of the C-terminal tail sequence I-X-V/I in the groove of the core formed by strands β 4 and β 8 (Fig. 5). The C-terminal tail of AAC_{59–163}, residues 157–163 having amino acid sequence RAIPVSR, is bound in a hydrophobic groove on top of a neighboring core (Fig. 5). The same is true for the C-terminal tail of ABC_{68–162}, residues 157–162 having amino acid sequence RTI-PIT. However, the surprising finding is that the directionality of the C-terminal tail with respect to the binding groove differs in AAC_{59–163} and ABC_{68–162}. This is possible because of the similar binding to the core of the two highly conserved hydrophobic side chains, adjacent to the central proline residue 160. These residues extend into the

core, locking the C-terminal tail in place (Fig. 5 and Supporting Information Fig. S6). Further stabilization of the C-terminal tail is by hydrogen bonding: AAC_{59–163} arginines 157 and 163 hydrogen bond to the side chain of glutamate 83 and backbone carbonyl of glutamine 126, respectively. The arginine (NH₂) 157 distance to glutamate (OE2) 83 is 3.7 Å. ABC_{68–162} arginine 157 hydrogen bonds with the backbone carbonyl of residue 131. The corresponding glutamate, AAC residue 83 is residue 87 in ABC and points in the same direction. The C-terminal tail, in both AAC_{59–163} and ABC_{68–162}, forms a total of six hydrogen bonds to β 4 and β 8. AAC_{59–163} forms three hydrogen bonds to β 8 and two hydrogen bonds to β 4, and ABC_{68–162} forms two hydrogen bonds to β 8 and three hydrogen bonds to β 4. Permitting the opposite directionality, the same hydrogen bonds are made on each side of the central proline residue.

Molecular basis for polydispersity

The molecular basis for polydispersity of the crystallins appears to be encoded in the palindromic nature of the C-terminal tail. Notice that the C-terminal tail,

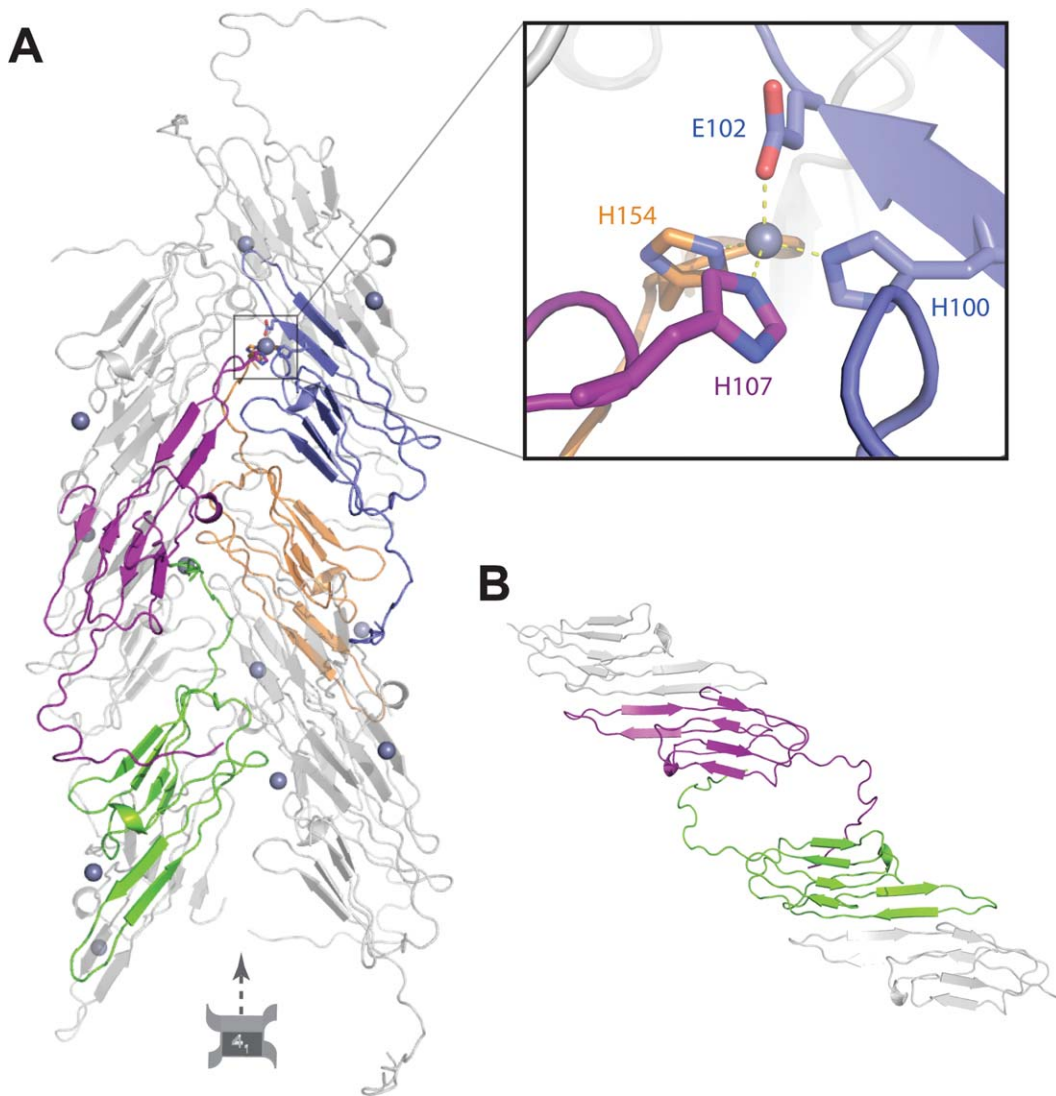


Figure 3. Zinc-bound crystal structure of AAC₅₉₋₁₆₃ and reciprocal C-terminal tail domain swap. (A) Crystallographic fourfold screw (winged square) axis is shown. Representative molecules involved in zinc binding are colored purple, blue, and green. The C-terminal domain swap of the green molecule is shown in purple. Zinc atoms are shown as gray spheres. The zinc-binding motif is created from residues of three different molecules. The inset shows a close-up view of the three histidines and one glutamate that make up the zinc-binding site. Residues are labeled and colored by atom type with carbon matching molecule color. (B) The C-terminal extension domain swaps reciprocate into each other, forming a closed domain swap. The C-terminal hinge forms a “w” like structure, which is discussed in the text. An [interactive view](#) is available in the electronic version of the article.

conserved among the crystallin protein family, is palindromic. The palindromic sequences, residues 156–164, in AAC and ABC, respectively, have amino acid sequence ERAIPVSRE and ERTIPITRE [Fig. 1(A)]. In addition to the palindromic sequence, the C-terminal tail has a pseudo-twofold axis centered on proline 160. By analyzing the crystallin family, we identified a conserved motif, E/D-R-X-I-P-V/I-X-R-E/D-E/D-K, containing this palindromic sequence. In contrast, WhHsp16.9³¹ and MjHsp16.5³² C-terminal domains lack this palindromic feature.

Polymeric assemblies AAC₅₉₋₁₆₃ and ABC₆₈₋₁₆₂ are formed by the domain swapping of the C-terminal extension. The C-terminal extension swap in

AAC₅₉₋₁₆₃ creates a polymer along a fourfold screw axis [Supporting Information Fig. S7(A,B)], and additional polymeric assemblies can be made for AAC₅₉₋₁₆₃, for example, along a twofold screw axis (shown in Fig. 2). Thus, in AAC₅₉₋₁₆₃, a complex network of C-terminal extension swaps is made. For AAC₅₉₋₁₆₃-Zn, a different C-terminal extension domain swapping arrangement is observed. The AAC₅₉₋₁₆₃-Zn C-terminal extension swaps in a reciprocal fashion [Fig. 3(B)]. This creates individual polymeric strands along the fourfold screw axis that twist together [Fig. 3(A)]. In our ABC₆₈₋₁₆₂ crystals, the C-terminal extension swapping of successive tails forms a runaway domain swap creating an

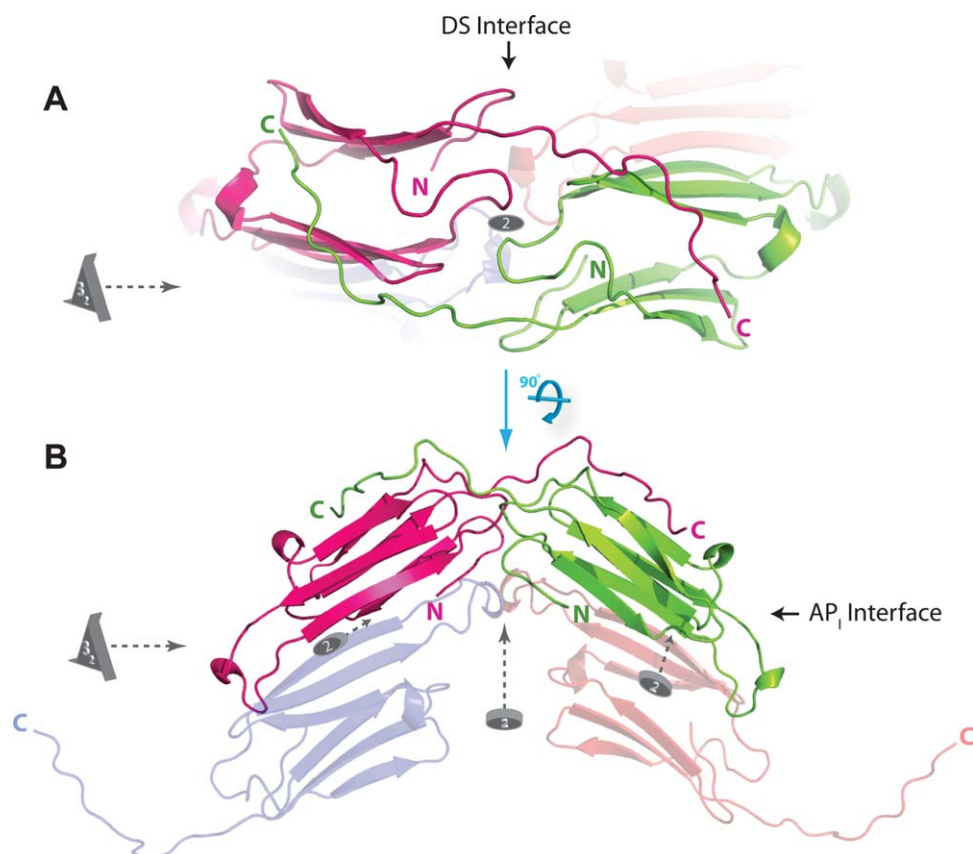


Figure 4. Crystal structure of ABC₆₈₋₁₆₂ reveals a domain swap of the C-terminal tail. Crystallographic axes and termini labels are shown as in Figure 3, with additional threefold screw (winged triangle) axes. (A) A dimeric interaction is created by swapping of the C-terminal tail from a neighboring molecule, which binds to the hydrophobic groove located on top of the core. (B) In addition to the domain-swapped dimeric interface (DS), a second dimeric interface (AP) is mediated through an antiparallel beta sheet. An [interactive view](#) is available in the electronic version of the article.

infinite noncovalent oligomer (Supporting Information Fig. S7(C,D)). This C-terminal extension swapping is reciprocal, similar to AAC₅₉₋₁₆₃-Zn.

AP interfaces in AAC₅₉₋₁₆₃ and ABC₆₈₋₁₆₂

A second type of interface is created by edge strands each of the antiparallel beta sheet, which we term AP. The AP dimers for AAC₅₉₋₁₆₃ and AAC₅₉₋₁₆₃-Zn have the same registration. A structural alignment of the AAC₅₉₋₁₆₃ dimer created by the AP interface with the dimer created by the AP interface of ABC₆₈₋₁₆₂ gives a C α backbone RMSD of 4.5 Å. Part of this large difference is the result of a shift in the registration of the AP interface in the ABC₆₈₋₁₆₂ structure, relative to the AAC₅₉₋₁₆₃ structure (Fig. 6 and Supporting Information Fig. S8). The registration shift in the ABC₆₈₋₁₆₂ AP interface is inward, molecules moving closer to each other, using the registration in AAC₅₉₋₁₆₃ structure as reference. Interestingly, a registration shift was also observed at the AP interface for the crystal structures of ABC₆₇₋₁₅₇ and Hsp20₆₅₋₁₆₂.²⁶ The AAC₅₉₋₁₆₃ structure exhibits the same registration as observed in ABC₆₇₋₁₅₇, whereas the registration shift for ABC₆₈₋₁₆₂ and Hsp20₆₅₋₁₆₂

is in opposite directions, inward and outward, respectively [Supporting Information Fig. S8(A,B)]. Establishing the most inward registration as the reference point, the three states for the outward registration translation of up to 15 Å are AP_I [ABC₆₈₋₁₆₂, presented here; Fig. 6(A)], AP_{II} [AAC₅₉₋₁₆₃, presented here; AAC₅₉₋₁₆₃-Zn, presented here; ABC₆₇₋₁₅₇²⁶; Fig. 6(B,C)], and AP_{III} [Hsp20₆₅₋₁₆₂²⁶; Fig. 6(D)]. The AP interface in Hsp20₆₅₋₁₆₂ is some 200 Å² greater in solvent-accessible surface area than in ABC₆₈₋₁₆₂ (Table II).

DS interface in ABC₆₈₋₁₆₂

Another dimer interface is observed only for ABC₆₈₋₁₆₂. This second dimer interface, which we term DS, is formed by the domain-swapped C-terminal extensions (Table II). The DS interface has ~600 Å² more buried area than the AP_I interface. In addition, two loops interact at the ABC₆₈₋₁₆₂ DS interface. Both loops are located along a crystallographic twofold axis [Fig. 4(A)]. The first loop, residues 123–128, and the second loop, residues 107–112, create the dimer interface. However, electron density is unclear for residues 106–109 in the dimer region

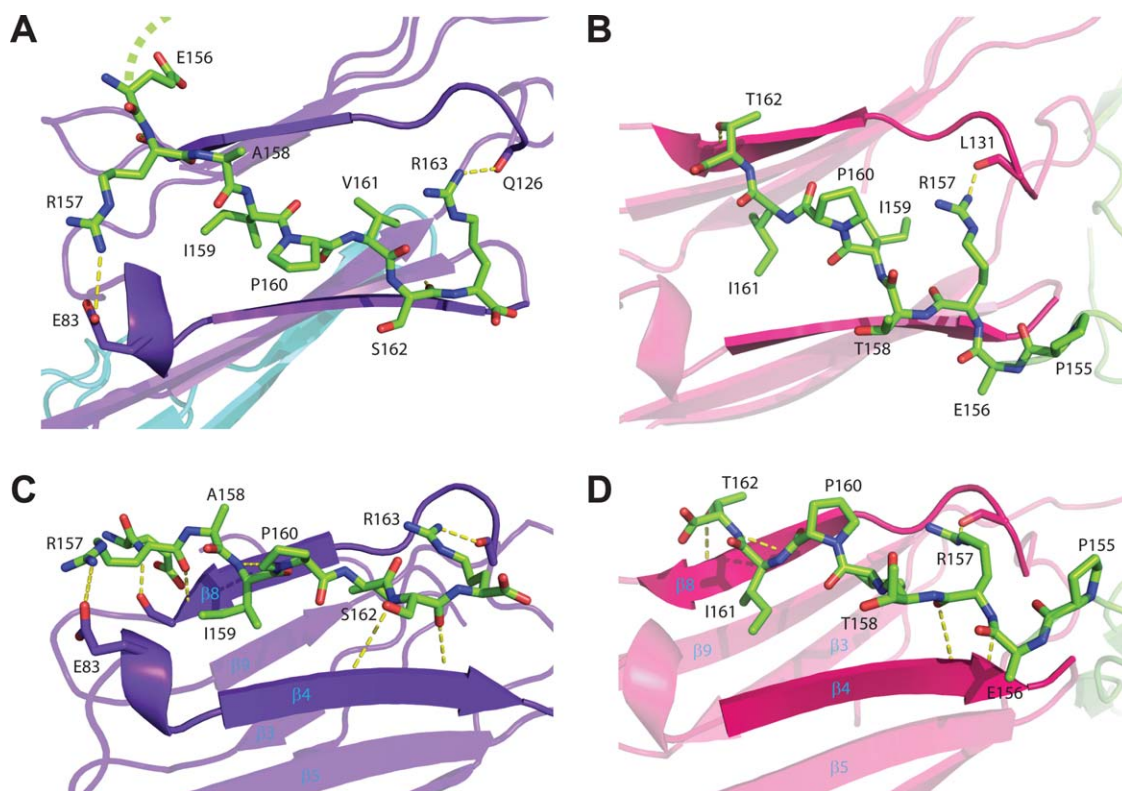


Figure 5. The C-terminal tail palindromic sequences allow bidirectional binding. The highly conserved tail motif of AAC and ABC bound in the hydrophobic groove created by beta strands $\beta 4$ and $\beta 8$. AAC_{59–163} and ABC_{68–162} C-terminal tail binding is shown in panels A, C and B, D, respectively. Panels B and D have the same orientations as A and B of Figure 4. Panels A and C have molecules oriented to match B and D. The tail, AAC_{59–163} residues 156–163 and ABC_{68–162} residues 155–162, containing the conserved motif is colored by atom type with carbon in green and the neighboring molecule is shown as purple (AAC_{59–163}) or pink (ABC_{68–162}) ribbon. Selected residues are labeled and hydrogen bonds shown by dashed yellow lines and discussed in the text. Beta strand are labeled in panels C, D. Both conserved hydrophobic residues in the C-terminal tail sequence (I-P-I/V) are buried into the hydrophobic core. The directionality of the C-terminal tail between AAC_{59–163} and ABC_{68–162} differs but maintain a pseudo twofold axis centered around proline 160. The palindromic sequence of the C-terminal tails, ERAIPVSRE (AAC_{59–163}) and ERTIPITRE (ABC_{68–162}), allow the bidirectional binding, while maintaining similar hydrogen bonding to the neighboring molecule. An [interactive view](#) is available in the electronic version of the article.

Discussion

The crystallins are the major proteins of the eye lens, the refractive power of which is achieved by their enormously high protein concentration (human ~ 400 mg/mL, rat ~ 900 mg/mL, and blue eyed trevally fish ~ 1100 mg/mL).^{42–47} Much study has been devoted to understanding how the lens remains transparent, despite its high protein concentrations.^{42–48} One factor is avoidance of phase separations within the lens, which would lead to light scattering and opacity, as in cataract formation. The common types of phase separation in protein solutions at high concentration are protein crystal formation and protein aggregation. The well-established chaperone function of alpha crystallin presumably protects against aggregation. Crystallization, so welcome to crystallographers and encouraged by them by concentrating protein solutions, destroys lens transparency and must be prevented in functional lenses.^{49,50} Although pure substances readily crystallize from solutions at high concentra-

tion, polydisperse and heterogeneous substances tend not to crystallize. As the most abundant lens proteins, crystallins might be expected to endanger transparency by spontaneous crystallization, and in fact, crystals of gamma-D-crystallin have been identified in one cataract.⁴⁹ Evolution of molecular mechanisms to ensure polydispersity of the crystallins would be one type of protection against lens crystallization.

Molecular mechanisms for enforcing polydispersity of crystallins

Alpha crystallin has evolved polymorphic interfaces: a bidirectional binding mode and multiple AP interface registrations, which act to frustrate formation of long-range order that could lead to crystalline domains (Fig. 7).

A bidirectional binding mode is encoded as a palindromic sequence in the alpha crystallin family [Fig. 1(A)]. The adaptation to a bidirectional binding mode enhances entropy and results in polydisperse

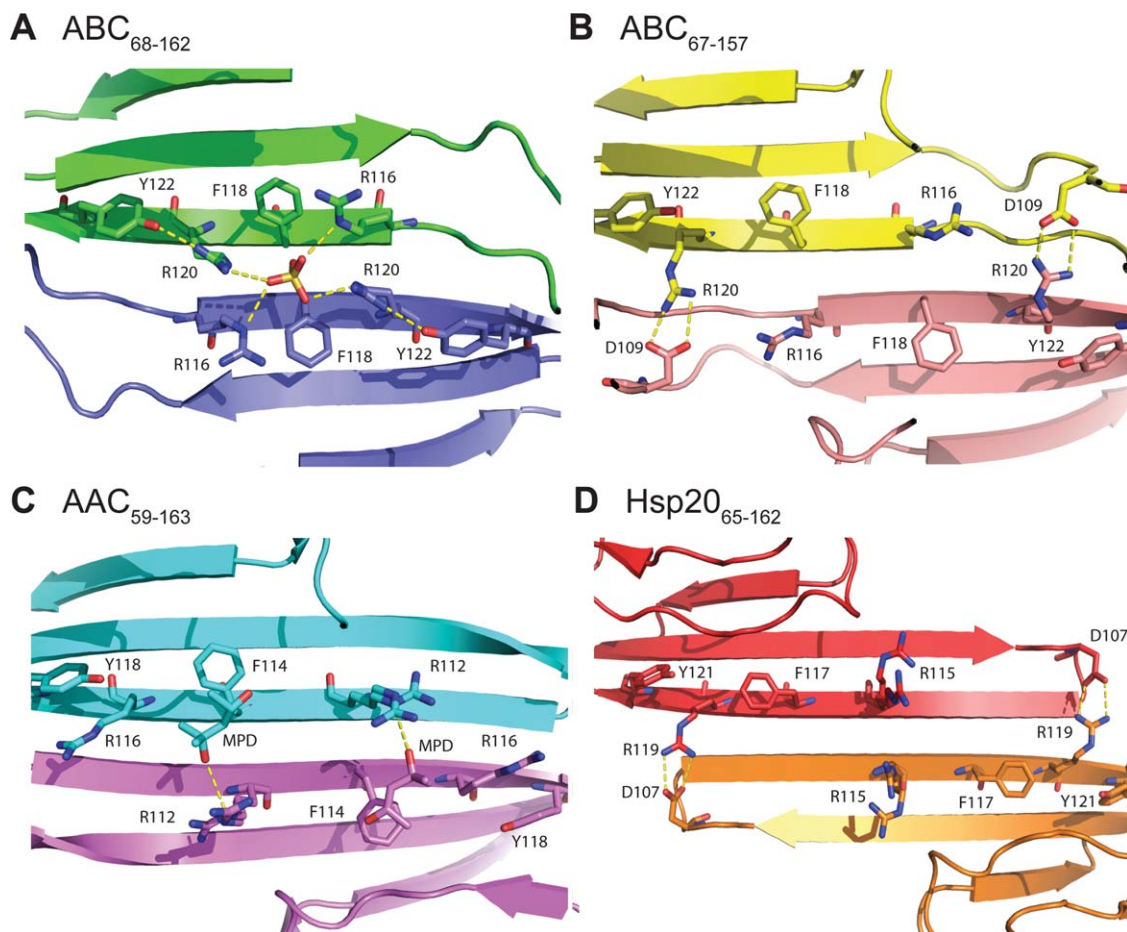


Figure 6. Registration shift within the AP interface for the alpha crystallin domain and implications for disease-related residues. Hydrogen bonds are shown by dashed yellow line. (A) The ABC₆₈₋₁₆₂ AP interface within the structure of this article containing the C-terminal extension (AP_I). A sulfate ion located on the twofold axis is surrounded by four arginine residues, acting as a hydrogen bond bridge between chains. Disease-related arginine 120 forms hydrogen bonds to tyrosine 123 and sulfate ion. (B) ABC₆₇₋₁₅₇,²⁶ lacking the C-terminal tail, AP interface (AP_{II}). Intersubunit hydrogen bonds are formed between arginine 120 and aspartate 109 from the other monomer. (C) The AAC₅₉₋₁₆₃ AP_{II} interface, with disease-related residues arginine 116 and tyrosine 118. (D) The Hsp20₆₅₋₁₆₂ AP_{III} interface. An [interactive view](#) is available in the electronic version of the article.

oligomers. Regardless of the directionality of the binding mode, the same number of hydrogen bonds is made to the alpha crystallin domain (Fig. 5), suggesting no enthalpic gain of one binding mode over the other. The increased entropy and roughly equal enthalpy for the two binding modes ensure that the alpha crystallins will be polydisperse in solution: the mixture must have lower free energy than either uniform dimer. This type of bidirectional binding would favor short-range interactions and disfavor long-range or crystalline-like order. In addition, a similar bidirectional interaction is observed for the N-terminal extension in Tsp36.³⁴ The N-terminal extension in AAC and ABC may have similar interactions, but Tsp36,³⁴ AAC, and ABC lack this palindromic feature. Assuming the N-terminal extension interacts in these various modes, it would further support polydispersity.

The polymorphic AP interfaces provide a structural mechanism not only for decreasing long-range

order but also could conceivably be involved in chaperone function. The different AP interfaces result in intermolecular shifts of up to 15 Å. The multiple interfaces, AP_{I-III}, create varying surface properties that presumably account for the assembly of alpha crystallin proteins into polydisperse oligomers. However, the polymorphic AP interfaces may also offer a clue to the structure-based function of substrate recognition and chaperone activity in AAC and ABC. These varied interfaces could represent functional states, for example, in a ratchet-based mechanism. The state of the ratchet could depend on concentrations of effectors or on other cellular conditions. It is unclear at this time whether multiple AP interfaces exist *in vivo*, but the ratchet-like AP interface could participate in chaperone activity as well as contributing to the polydispersity that prevents crystallization within the lens.

A second molecular feature that ensures polymorphic oligomeric assemblies of AAC and ABC is

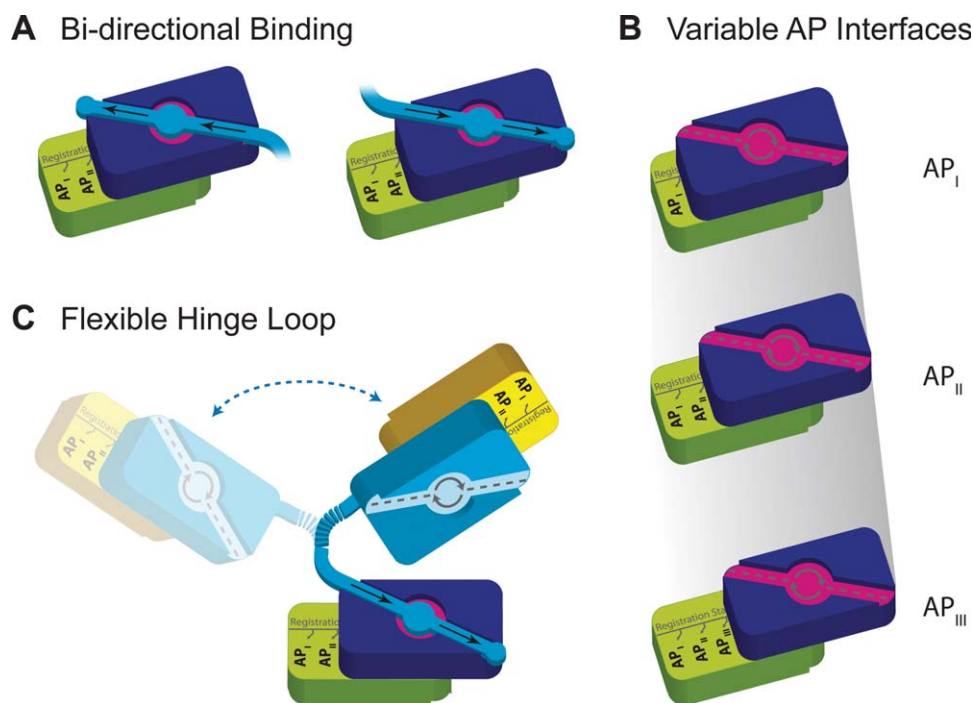


Figure 7. Summary of alpha crystallin structural mechanisms of polydispersity. Alpha crystallin molecules are represented by square boxes. The C-terminal extension is shown for molecules colored in light blue with arrows indicating N- to C-termini directionality. The binding groove for the C-terminal extension is shown by a recessed groove. (A) Bidirectional binding of the C-terminal extension is highlighted in the binding groove by dashed lines and turning solid arrows. The two orientations of the bound C-terminal extension are shown. The circle, located between the two C-terminal extension directionality arrows, indicates the pseudo twofold axis. (B) The three registration states located on the AP interface. The registration state is labeled to the right. (C) The flexible hinge loop allows variable states for the C-terminal extension to bind to neighboring molecules. The blue dashed line indicates the flexibility in the hinge loop. The AP_{II} interface is shown in panels A and C; however, the other two states could apply as well. Accounting for just the bidirectional binding and variable AP interfaces, a total of 108 possible oligomeric states exist for a hexamer. The large polydisperse oligomers, for example of 20 molecules, 30,233,088 oligomeric states exist. How all these diverse states participate in chaperone function is unclear. These polymorphic interfaces disfavor crystallization and hence remove one factor that could diminish transparency.

the flexible hinge loop that permits C-terminal tail bidirectional binding (Supporting Information Fig. S5). Flexibility allows the alpha crystallin molecules to interact in a variety of modes and to binding to neighboring molecules via the palindromic sequences [Fig. 1(A)]. Flexibility is not surprising, because this was also observed in the C-terminal extension of WhHsp16.9.³¹ Further support of a flexible hinge loop comes from an engineered MjHsp16.5 protein, where the flexible hinge loop of the C-terminal extension enables repacking of larger symmetrical oligomer.¹⁹ Furthermore, the flexibility in the hinge loop could support binding to its own domain, thus not forming a domain swap. In addition, the presence of Zn may not be the determinant of C-terminal extension direction in AAC. Taken together, the flexible hinge loop and palindromic C-terminal tail sequences promote polydisperse interactions.

Polydispersity of truncated alpha crystallins

Truncated alpha crystallin proteins display the polydisperse properties of their full-length parents. The

discrete dimeric steps in molecular mass (Fig. 1) most likely originate from the dimeric unit created by the AP interface. The observed polydispersity within these discrete molecular groupings presumably arises from C-terminal tail interactions. As protein concentration increases, the C-terminal tail binding is favored promoting the formation of tetrameric and hexameric assemblies. The population of large polydisperse oligomers resembles that of the full-length molecules, with similar subunit distributions.^{18,22,40} Although the relative abundance of these large polydisperse oligomers of truncated molecules is low, the sensitivity of the MS technique over other techniques, such as light scattering, permits their detection. Although the truncation of N-terminal residues was necessary to obtain crystals (this article, Refs. 26 and 51), these truncated proteins lead to destabilization of the large polydisperse oligomer species and favor smaller oligomeric species (monomers, dimers, tetramers, and hexamers) that allow for crystal growth. These suboligomeric species outweigh the large polydisperse oligomer population,

Table I. X-Ray Data Collection and Refinement Statistics for Truncated AlphaA (AAC₅₉₋₁₆₃), Zinc-Bound tAAC (AAC₅₉₋₁₆₃-Zn), and AlphaB (ABC₆₈₋₁₆₂) Crystallin

	AAC ₅₉₋₁₆₃	AAC ₅₉₋₁₆₃ -Zn	AAC ₅₉₋₁₆₃ -Zn	ABC ₆₈₋₁₆₂
Crystal parameters				
Space group	P4 ₁ 2 ₁ 2	P4 ₁ 2 ₁ 2	P4 ₁ 2 ₁ 2	P3 ₂ 12
Unit cell dimensions (Å)	$a = 56.06, b = 56.06, c = 69.26$	$a = 56.21, b = 56.21, c = 68.66$	$a = 56.21, b = 56.21, c = 68.65$	$a = 50.95, b = 50.95, c = 104.43$
Angles (°)	$\alpha = \beta = \gamma = 90$	$\alpha = \beta = \gamma = 90$	$\alpha = \beta = \gamma = 90$	$\alpha = \beta = 90, \gamma = 120$
Data collection				
Synchrotron (beamline)	ALS (8.2.1)	APS (24-ID-C)	APS (24-ID-C)	APS (24-ID-C)
λ (Å)	1.00	0.979	1.28	1.49
Resolution (Å)	39.64–1.53	25.98–1.15	43.49–1.50	18.8–3.32
R_{fac} (%) ^a	4.1 (49.6)	5.3 (40.3)	4.8 (30.5)	
$R_{\text{mrgd-F}}$ (%) ^b				6.1 (36.6)
I/σ	31.5 (3.2)	25.3 (3.4)	29.5 (3.7)	21.2 (5.3)
Reflections observed/unique	111962/16465	218757/36986	135178/17697	13703/2379
Completeness (%)	95 (99)	93 (92)		98 (100)
Anomalous completeness (%)			97 (86)	
Refinement				
R_{work} (%)	18.9	16.4		29.8
R_{free} (%)	21.0 ^c	19.3 ^c		32.7 ^d
Number of protein atoms	801	892		749
Nonprotein atoms	8	7		10
Number of water molecules	43	95		0
RMSD bond/angle (Å/°)	0.005/1.05	0.007/1.227		0.007/1.218
Wilson B-factor (Å ²)	24	9		104 ^e
B factor of protein atoms	28	12		166 ^e
Ramachandran map, favored/outlier (%)	93/7	91/9		67/26
PDB accession code	3L1F	3L1E		3L1G

Values in parentheses correspond to the highest resolution shell.

^a $R_{\text{fac}} = \sum |I - \langle I \rangle| / \sum I$.

^b $R_{\text{mrgd-F}} = (\sum |A_{I(h,p)} - A_{I(h,q)}|) / (0.5 * \sum A_{I(h,p)} + A_{I(h,q)})$, where $A_I = (\sqrt{I}$ if $I \geq 0$ or $-\sqrt{I}$ if $I < 0$) as described.⁵²

^c R_{free} calculated using 5% of the data.

^d R_{free} calculated using 10% of the data.

^e Crystals were anisotropic (Supporting Information Fig. S12).

reversing the equilibrium in comparison to their full-length parent proteins. The shift in equilibrium suggests that the truncated N-terminal residues confer additional stability to the large polydisperse oligomer assemblies. The truncated proteins display a similar pattern of oligomerization, assembly, and self-association to their parent proteins.

Material and Methods

Protein expression

AAC₅₉₋₁₆₃, ABC₆₈₋₁₆₂, ABC₆₈₋₁₆₂ R157H, and ABC₆₈₋₁₅₇ were expressed with TEV protease cleavable N-terminal His-tags from pET28b (Novagen, Gibbstown, NJ). All proteins were expressed in Rosetta 2 (DE3) cells (Novagen, Gibbstown, NJ). Proteins were purified by affinity chromatography, followed by TEV protease cleavage of N-terminal His-tag, and final purification by gel filtration chromatography (Supporting Information Experimental Procedures).

Data collection and structure determination

Crystals were grown in hanging drop or sitting drop plates. AAC₅₉₋₁₆₃-Zn (cryoprotected), AAC₅₉₋₁₆₃ (cry-

oprotected), and ABC₆₈₋₁₆₂ crystals were flash frozen in liquid nitrogen for data collection at ALS and APS (Table I). Experimental phases for AAC₅₉₋₁₆₃-Zn were determined, followed by automated and manual model building. The AAC₅₉₋₁₆₃ and ABC₆₈₋₁₆₂ structures were determined by molecular replacement, followed by automated and manual model building. The details are provided in Supporting Information Experimental Procedures.

Table II. Summary of Buried Solvent-Accessible Areas for DS and AP_{I-III} Interfaces in AAC₅₉₋₁₆₃, ABC₆₈₋₁₆₂, ABC₆₇₋₁₅₇, and Hsp20₆₅₋₁₆₂

Protein	Interface area buried (Å ²) ^a	Interface
AAC ₅₉₋₁₆₃	644	AP _{II}
	505	C-terminal tail
ABC ₆₈₋₁₆₂	1304	DS
	785	AP _I
ABC ₆₇₋₁₅₇	633 ^b	AP _{II}
Hsp20 ₆₅₋₁₆₂	571	AP _{III}

^a Calculated using PISA, as described in material and methods, and reported as interface area buried per chain.

^b Average value reported.

Structure analysis

Surface area was calculated using PISA.^{53,54} Shape complementarity was calculated using SC^{54,55} distributed by CCP4.⁵⁶

Electrospray MS

Nanoelectrospray MS was performed on a Q-ToF 2 mass spectrometer (Waters, Milford, MA) as previously described.²¹ For all spectra, protein samples were in 200 mM ammonium acetate, pH 6.9.

Chaperone activity assays

All chaperone assays were performed as previously described.⁵⁷ Further details are described in the Supporting Information Experimental Procedures.

Conclusions

The results of our work suggest that alpha crystallin proteins have evolved a structure-based mechanism of polydispersity that is one factor in supporting the lens function of transparency.^{42,43,47–49,58} Both the AP interface and the C-terminal tail interactions observed for the alpha crystallin family exhibit structural polymorphisms (Fig. 7). The ratchet-like AP interface gives rise to three differing interface registers, which vary in area buried but maintain the same total number of hydrogen bonds between chains. A conserved palindromic sequence supports bidirectional C-terminal tail binding modes, which maintain the same number of hydrogen bonds. The flexible hinge loop permits this bidirectional binding. The polymorphic nature that we have observed at both common interfaces formed by truncated alpha crystallins provides the structural mechanism of polydispersity for the full-length crystallins to ensure polymorphic oligomeric structures.

Acknowledgments

The authors thank Christine Slingsby for sending PDB coordinates prior to PDB release, Paul Muchowski and John Clark for useful discussion, Mark Arbing for advice and TEV plasmid, Daniel Anderson for crystallization tips and advice, Douglas Rees for summer CBI internship and discussion, UCLA-DOE X-ray Crystallography Core Facility, Jason Navarro at the UCLA Crystallization Facility, Corie Ralston for help with X-ray data collection at ALS beamline 8.2.1, ALS and BCSB, M. Capel, K. Rajashankar, F. Murphy, J. Schuermann, and I. Kourinov at NE-CAT beamline 24-ID-C at APS.

References

1. McHaourab HS, Godar JA, Stewart PL (2009) Structure and mechanism of protein stability sensors: chaperone activity of small heat shock proteins. *Biochemistry* 48: 3828–3837.
2. Ghosh JG, Houck SA, Clark JI (2008) Interactive sequences in the molecular chaperone, human alphaB

crystallin modulate the fibrillation of amyloidogenic proteins. *Int J Biochem Cell Biol* 40:954–967.

3. Horwitz J (1992) Alpha-crystallin can function as a molecular chaperone. *Proc Natl Acad Sci USA* 89: 10449–10453.
4. Rekas A, Jankova L, Thorn DC, Cappai R, Carver JA (2007) Monitoring the prevention of amyloid fibril formation by alpha-crystallin. Temperature dependence and the nature of the aggregating species. *FEBS J* 274:6290–6304.
5. Tanaka N, Tanaka R, Tokuhara M, Kunugi S, Lee YF, Hamada D (2008) Amyloid fibril formation and chaperone-like activity of peptides from alphaA-crystallin. *Biochemistry* 47:2961–2967.
6. Treweek TM, Ecroyd H, Williams DM, Meehan S, Carver JA, Walker MJ (2007) Site-directed mutations in the C-terminal extension of human alphaB-crystallin affect chaperone function and block amyloid fibril formation. *PLoS ONE* 2:e1046.
7. Ecroyd H, Carver JA (2009) Crystallin proteins and amyloid fibrils. *Cell Mol Life Sci* 66:62–81.
8. Muchowski PJ, Wacker JL (2005) Modulation of neurodegeneration by molecular chaperones. *Nat Rev Neurosci* 6:11–22.
9. Sun Y, MacRae TH (2005) The small heat shock proteins and their role in human disease. *FEBS J* 272: 2613–2627.
10. Renkawek K, de Jong WW, Merck KB, Frenken CW, van Workum FP, Bosman GJ (1992) Alpha B-crystallin is present in reactive glia in Creutzfeldt-Jakob disease. *Acta Neuropathol* 83:324–327.
11. Goldman JE, Corbin E (1991) Rosenthal fibers contain ubiquitinated alpha B-crystallin. *Am J Pathol* 139: 933–938.
12. Lowe J, McDermott H, Pike I, Spendlove I, Landon M, Mayer RJ (1992) alpha B crystallin expression in non-lenticular tissues and selective presence in ubiquitinated inclusion bodies in human disease. *J Pathol* 166:61–68.
13. Renkawek K, Stege GJ, Bosman GJ (1999) Dementia, gliosis and expression of the small heat shock proteins hsp27 and alpha B-crystallin in Parkinson's disease. *Neuroreport* 10:2273–2276.
14. Renkawek K, Voorter CE, Bosman GJ, van Workum FP, de Jong WW (1994) Expression of alpha B-crystallin in Alzheimer's disease. *Acta Neuropathol* 87:155–160.
15. de Jong WW, Caspers GJ, Leunissen JA (1998) Genealogy of the alpha-crystallin-small heat-shock protein superfamily. *Int J Biol Macromol* 22:151–162.
16. de Jong WW, Leunissen JA, Voorter CE (1993) Evolution of the alpha-crystallin/small heat-shock protein family. *Mol Biol Evol* 10:103–126.
17. Klemenz R, Frohli E, Steiger RH, Schafer R, Aoyama A (1991) Alpha B-crystallin is a small heat shock protein. *Proc Natl Acad Sci USA* 88:3652–3656.
18. Aquilina JA, Benesch JL, Bateman OA, Slingsby C, Robinson CV (2003) Polydispersity of a mammalian chaperone: mass spectrometry reveals the population of oligomers in alphaB-crystallin. *Proc Natl Acad Sci USA* 100:10611–10616.
19. Shi J, Koteiche HA, McHaourab HS, Stewart PL (2006) Cryoelectron microscopy and EPR analysis of engineered symmetric and polydisperse Hsp16.5 assemblies reveals determinants of polydispersity and substrate binding. *J Biol Chem* 281:40420–40428.
20. Horwitz J (2003) Alpha-crystallin. *Exp Eye Res* 76: 145–153.
21. Benesch JL, Ayoub M, Robinson CV, Aquilina JA (2008) Small heat shock protein activity is regulated by variable oligomeric substructure. *J Biol Chem* 283: 28513–28517.

22. Aquilina JA, Benesch JL, Ding LL, Yaron O, Horwitz J, Robinson CV (2005) Subunit exchange of polydisperse proteins: mass spectrometry reveals consequences of alphaA-crystallin truncation. *J Biol Chem* 280:14485–14491.
23. Haley DA, Horwitz J, Stewart PL (1998) The small heat-shock protein, alphaB-crystallin, has a variable quaternary structure. *J Mol Biol* 277:27–35.
24. Peschek J, Braun N, Franzmann TM, Georgalis Y, Haslbeck M, Weinkauff S, Buchner J (2009) The eye lens chaperone alpha-crystallin forms defined globular assemblies. *Proc Natl Acad Sci USA* 106:13272–13277.
25. Horwitz J, Huang Q, Ding L (2004) The native oligomeric organization of alpha-crystallin, is it necessary for its chaperone function? *Exp Eye Res* 79:817–821.
26. Bagneris C, Bateman OA, Naylor CE, Cronin N, Boelens WC, Keep NH, Slingsby C (2009) Crystal structures of alpha-crystallin domain dimers of alphaB-crystallin and Hsp20. *J Mol Biol* 392:1242–1252.
27. Berengian AR, Bova MP, McHaourab HS (1997) Structure and function of the conserved domain in alphaA-crystallin. Site-directed spin labeling identifies a beta-strand located near a subunit interface. *Biochemistry* 36:9951–9957.
28. Berengian AR, Parfenova M, McHaourab HS (1999) Site-directed spin labeling study of subunit interactions in the alpha-crystallin domain of small heat-shock proteins. Comparison of the oligomer symmetry in alphaA-crystallin, HSP 27, and HSP 16.3. *J Biol Chem* 274:6305–6314.
29. Jehle S, van Rossum B, Stout JR, Noguchi SM, Falber K, Rehbein K, Oschkinat H, Klevit RE, Rajagopal P (2009) alphaB-crystallin: a hybrid solid-state/solution-state NMR investigation reveals structural aspects of the heterogeneous oligomer. *J Mol Biol* 385:1481–1497.
30. Koteiche HA, Berengian AR, McHaourab HS (1998) Identification of protein folding patterns using site-directed spin labeling. Structural characterization of a beta-sheet and putative substrate binding regions in the conserved domain of alpha A-crystallin. *Biochemistry* 37:12681–12688.
31. van Montfort RL, Basha E, Friedrich KL, Slingsby C, Vierling E (2001) Crystal structure and assembly of a eukaryotic small heat shock protein. *Nat Struct Biol* 8:1025–1030.
32. Kim KK, Kim R, Kim SH (1998) Crystal structure of a small heat-shock protein. *Nature* 394:595–599.
33. Hilario E, Teixeira EC, Pedrosa GA, Bertolini MC, Medrano FJ (2006) Crystallization and preliminary X-ray diffraction analysis of XAC1151, a small heat-shock protein from *Xanthomonas axonopodis* pv. citri belonging to the alpha-crystallin family. *Acta Crystallogr Sect F Struct Biol Cryst Commun* 62:446–448.
34. Stamler R, Kappe G, Boelens W, Slingsby C (2005) Wrapping the alpha-crystallin domain fold in a chaperone assembly. *J Mol Biol* 353:68–79.
35. Alexander N, Bortolus M, Al-Mestarihi A, McHaourab H, Meiler J (2008) De novo high-resolution protein structure determination from sparse spin-labeling EPR data. *Structure* 16:181–195.
36. Bloemendal H, de Jong W, Jaenicke R, Lubsen NH, Slingsby C, Tardieu A (2004) Ageing and vision: structure, stability and function of lens crystallins. *Prog Biophys Mol Biol* 86:407–485.
37. Li Y, Schmitz KR, Salerno JC, Koretz JF (2007) The role of the conserved COOH-terminal triad in alphaA-crystallin aggregation and functionality. *Mol Vis* 13:1758–1768.
38. Pasta SY, Raman B, Ramakrishna T, Rao ChM (2004) The IXI/V motif in the C-terminal extension of alpha-crystallins: alternative interactions and oligomeric assemblies. *Mol Vis* 10:655–662.
39. Ghosh JG, Shenoy AK, Jr, Clark JI (2006) N- and C-Terminal motifs in human alphaB crystallin play an important role in the recognition, selection, and solubilization of substrates. *Biochemistry* 45:13847–13854.
40. Benesch JL, Aquilina JA, Ruotolo BT, Sobott F, Robinson CV (2006) Tandem mass spectrometry reveals the quaternary organization of macromolecular assemblies. *Chem Biol* 13:597–605.
41. Kleywegt GJ (1999) Recognition of spatial motifs in protein structures. *J Mol Biol* 285:1887–1897.
42. Benedek G (1983) Why the eye lens is transparent. *Nature* 302:383–384.
43. Delaye M, Tardieu A (1983) Short-range order of crystallin proteins accounts for eye lens transparency. *Nature* 302:415–417.
44. Philipson B (1969) Distribution of protein within the normal rat lens. *Invest Ophthalmol* 8:258–270.
45. Pierscionek BK, Augusteyn RC (1995) The refractive index and protein distribution in the blue eye trevally lens. *J Am Optom Assoc* 66:739–743.
46. Pierscionek BK, Chan DY (1989) Refractive index gradient of human lenses. *Optom Vis Sci* 66:822–829.
47. Veretout F, Delaye M, Tardieu A (1989) Molecular basis of eye lens transparency. Osmotic pressure and X-ray analysis of alpha-crystallin solutions. *J Mol Biol* 205:713–728.
48. Xia JZ, Wang Q, Tatarkova S, Aerts T, Clauwaert J (1996) Structural basis of eye lens transparency: light scattering by concentrated solutions of bovine alpha-crystallin proteins. *Biophys J* 71:2815–2822.
49. Kmoch S, Brynda J, Asfaw B, Bezouska K, Novak P, Rezacova P, Ondrova L, Filipec M, Sedlacek J, Elleder M (2000) Link between a novel human gammaD-crystallin allele and a unique cataract phenotype explained by protein crystallography. *Hum Mol Genet* 9:1779–1786.
50. Brooks DG, Manova-Todorova K, Farmer J, Lobmayr L, Wilson RB, Eagle RC, Jr, St Pierre TG, Stambolian D (2002) Ferritin crystal cataracts in hereditary hyperferritinemia cataract syndrome. *Invest Ophthalmol Vis Sci* 43:1121–1126.
51. Baranova EV, Beelen S, Gusev NB, Strelkov SV (2009) The taming of small heat-shock proteins: crystallization of the α -crystallin domain from human Hsp27. *Acta Crystallogr Sect F Struct Biol Cryst Commun* 65:1277–1281.
52. Kabsch W (1993) Automatic processing of rotation diffraction data from crystals of initially unknown symmetry and cell constants. *J Appl Crystallogr* 26:795–800.
53. Krissinel E (2010) Crystal contacts as nature's docking solutions. *J Comput Chem* 31:133–143.
54. Krissinel E, Henrick K (2007) Inference of macromolecular assemblies from crystalline state. *J Mol Biol* 372:774–797.
55. Lawrence MC, Colman PM (1993) Shape complementarity at protein/protein interfaces. *J Mol Biol* 234:946–950.
56. CCP4 (1994) The CCP4 suite: programs for protein crystallography. *Acta Crystallogr D Biol Crystallogr* 50:760–763.
57. Horwitz J, Alpha-crystallin: its involvement in suppression of protein aggregation and protein folding. In: Buchner J, Kiefhaber T, Eds. (2005) Protein folding handbook Part II. Weinheim, Germany: Wiley-VCH, pp 858–875.
58. Benedek GB (1971) Theory of transparency of the eye. *Appl Opt* 10:459–473.